Contents lists available at ScienceDirect

Acta Materialia

journal homepage: www.elsevier.com/locate/actamat

CrossMark

Full length article

Computational and experimental studies on structure and mechanical properties of Mo−Al−N

F.F. Klimashin*, H. Euchner, P.H. Mayrhofer

Institute of Materials Science and Technology, Technische Universität Wien, Getreidemarkt 9, 1060, Vienna, Austria

A R T I C L E   I N F O

A B S T R A C T

Ab initio calculations show that with increasing N-vacancy content of $Mo_{1-x}Al_xN_y$ solid solutions, the cubic structure is increasingly preferred over the wurtzite-type hexagonal structure. While $Mo_{1-x}Al_xN$ solid solutions, without N-vacancies, energetically favor the wurtzite-type structure over the whole composition range, $Mo_{1-x}Al_xN_{0.5(1+x)}$ and $Mo_{1-x}Al_xN_{0.5}$ solid solutions energetically prefer the cubic structure up to ~45 and 65 at.% Al at the metal sublattice.

Detailed ab initio calculations in combination with detailed elemental and phase composition analyses and nanoindentation experiments of reactively sputtered $Mo_{1-x}Al_xN_y$ coatings prove the formation of face-centered cubic structures for Al-contents $x \leq 0.57$. These $Mo_{1-x}Al_xN_y$ coatings exhibit an Al-dependent population of the nitrogen sublattice, following the $MoN_{0.5}$−AlN quasi-binary tie line. For Al-contents $x \geq 0.79$ the coatings crystallize in the wurtzite-type hexagonal phase, while in the intermediate composition range both phases, cubic and wurtzite-type hexagonal, coexist. As long as the cubic structure is maintained, the hardness increases from ~33.0 to 38.4 GPa with increasing Al-content, but drops to ~22 GPa for $x \geq 0.67$, when the films contain hexagonal wurtzite-type phases.

1. Introduction

Face-centered cubic-structured γ-Mo_2N (B1, NaCl-type with half-populated N-sublattice, hence, actually $MoN_{0.5}$ [1]) exhibits excellent mechanical and tribological properties [2] and is therefore an ideal candidate for wear-resistant coatings. The major limitation of Mo−N coatings is their low resistance against oxidation, resulting in the formation of molybdenum oxides having a high vapour pressure [3]. To overcome these limitations, we have developed Mo−Al−N coatings, since Al typically increases the oxidation resistance of transition metal (TM) nitrides by forming dense oxides. Moreover, an increasing Al-content is known to improve the tribological and mechanical properties of TM nitrides by solid solution strengthening and age hardening [4−9]. Although the binary phases γ-Mo_2N and hexagonal-structured (ZnS wurtzite-type) w-AlN are not miscible in thermodynamic equilibrium, $Mo_{1-x}Al_xN$ solid solutions can be prepared by physical vapour deposition. Since the face-centered cubic-structured (c-) modification of AlN is a highly unstable high-pressure allotrope of the thermodynamically stable w-AlN structure [10], we expect the Al-content to play a crucial role in the formation of cubic-structured c-$Mo_{1-x}Al_xN_y$ and wurtzite-type w-$Mo_{1-x}Al_xN_y$ phases, similar to the cases of $Ti_{1-x}Al_xN$ [11−13] and $Cr_{1-x}Al_xN$ [13−15].

There is only a limited number of studies on coatings within the Mo−Al−N system and the reported maximum Al-content, $x = $ Al/(Mo + Al), achieved within single-phased c-$Mo_{1-x}Al_xN_y$ coatings is x ~0.3 [16−18]. Two recent publications even present deteriorating mechanical properties with increasing Al-content [17,18]. This rather unusual behavior and the limited information about sputtered Mo−Al−N coatings available, motivated us for a detailed study of this material system.

By combining ab initio and experimental studies of $Mo_{1-x}Al_xN_y$ we show that the metal sublattice population as well as the nitrogen sublattice population is crucial for the formation of face-centered cubic-structured solid solutions. Our experimental investigations clearly evidence that sputter-deposited $Mo_{1-x}Al_xN_y$ coatings with a face-centered cubic structure and chemical compositions close to the $MoN_{0.5}$−AlN quasi-binary tie line exhibit strongly improved mechanical properties with increasing aluminum content.

* Corresponding author.
E-mail address: fedor.klimashin@tuwien.ac.at (F.F. Klimashin).

2. Computational and experimental details

The respective energetic stability of face-centered cubic (c-) and hexagonal wurtzite-type (w-) solid solutions along the three quasi-binary tie lines, MoN—AlN, $MoN_{0.5}$—AlN, and $MoN_{0.5}$—$AlN_{0.5}$, was calculated using density functional theory (DFT) as implemented in the Vienna Ab initio Simulation Package (VASP) [19,20].

The energy of formation, E_f, was determined with respect to the elemental constituents, fcc-Al, bcc-Mo and molecular nitrogen, applying the following Eq. (1) [21]:

$$E_f = \frac{1}{\sum_i n_i}\left(E_{tot} - \sum_i n_i E_i\right) \tag{1}$$

Here E_{tot} and E_i are the total energy of the compound and its elemental constituents, respectively, as determined from DFT, while n_i denotes the number of atoms of species i. For a stability comparison between different structure types the configurational entropy can be neglected, since at a given concentration the configurational entropy is the same and independent of the structure type. Supercells with different chemical compositions were constructed using the special quasi-random structure (SQS) approach [22]. The high cooling rates in PVD and the fact that no heat treatment was applied, in combination with the absence of super-structure reflections in our XRD data, make ordering rather unlikely. Therefore, ordering tendencies were not investigated in our simulations. Wurtzite-type phases were studied with $2 \times 2 \times 4$ supercells using a $6 \times 6 \times 4$ kpoint mesh. The cubic phases were investigated with a $2 \times 2 \times 1$ supercell (along the MoN—AlN and $MoN_{0.5}$—AlN tie lines) and $2 \times 2 \times 2$ supercells (along the $MoN_{0.5}$—$AlN_{0.5}$ tie line) using $4 \times 4 \times 8$ and $4 \times 4 \times 4$ kpoint meshes, respectively. All computations were performed with the projector augmented wave method and the generalized gradient approximation (PAW-GGA) using an energy cutoff of 700 eV. Together with the chosen kpoint mesh, these settings guaranteed for an accuracy of a few meV/atom.

A modified Leybold Heraeus magnetron sputtering system Z400 was used to deposit Mo—Al—N thin films in Ar and N_2 atmosphere (purity above 99.999% for both gases). Mo-rich Mo—Al—N thin films were synthesised from a molybdenum target (99.97% purity, Ø75 mm) by covering the race track with different numbers of small Al-cubes (99.85% purity, $3 \times 3 \times 3$ mm^3). Al-rich Mo—Al—N coatings were prepared from an aluminum target (99.5% purity, Ø75 mm), where small Mo-cubes (99.99% purity, $3 \times 3 \times 3$ mm^3) uniformly covered the race track. Primarily to the deposition processes, the chamber was evacuated to a high vacuum of p_{base} ≤5·10⁻⁴ Pa. The sputter depositions were performed with a constant total pressure, p_T, of 0.35 Pa and a N_2-to-total pressure ratio of $p_{N2}/p_T = 0.32$, based on our previous study [1]. All depositions were carried out with a target current of 0.4 A DC while keeping the substrates at floating potential (~-15 V) and at 450 ± 20 °C.

The crystal structures of the as-deposited thin films were analyzed by X-ray diffraction (XRD), using a Philips X'Pert diffractometer with monochromatic Cu $K\alpha$ radiation in Bragg Brentano geometry. The stress-free lattice parameters were obtained with the "$\sin^2\psi$" method [23] using a PANalytical Empyrion diffractometer in glancing angle mode with an angle of incidence $\gamma = 2°$.

The film growth morphology was investigated by scanning electron microscopy (SEM) of fracture cross-sections. Energy dispersive X-ray spectroscopy (EDS) allowed for a chemical characterization of the thin films. The EDS measurements were calibrated with Mo—N thin film standards that have been characterized by elastic recoil detection analyses [1]. Mechanical properties, such as indentation modulus and hardness were determined by nano-indentation using an ultra micro indentation system (UMIS)

equipped with a Berkovich type indenter. The obtained load—displacement curves were evaluated after Oliver and Pharr [24] as described in detail in Refs. [1] and [25].

3. Results

Fig. 1a, b, and c present the energy of formation, E_f, of $Mo_{1-x}Al_xN_y$ with face-centered cubic (red squares) and wurtzite-type (green hexagons) crystal structures along the three quasi-binary tie lines, MoN—AlN, $MoN_{0.5}$—AlN, and $MoN_{0.5}$—$AlN_{0.5}$, respectively. Solid solutions along the MoN—AlN quasi-binary tie line, hence, with fully occupied N-sublattices, energetically prefer the wurtzite-type structure, w-$Mo_{1-x}Al_xN$, over the whole composition range, see Fig. 1a. Solid solutions along the $MoN_{0.5}$—AlN tie line exhibit a crossover between cubic- and wurtzite-type $Mo_{1-x}Al_xN_{0.5(1+x)}$ at Al-contents of x ~0.45 (see Fig. 1b), where lower Al-contents favor the cubic structure. Compositions along the $MoN_{0.5}$—$AlN_{0.5}$ tie line, hence, with half-occupied N-sublattices over the whole composition range, provide a crossover between cubic-structured and wurtzite-type $Mo_{1-x}Al_xN_{0.5}$ at x ~0.65.

The energies of formation for the cubic and wurtzite-type solid solutions $Mo_{1-x}Al_xN$, $Mo_{1-x}Al_xN_{0.5(1+x)}$, and $Mo_{1-x}Al_xN_{0.5}$, are very similar over a wide concentration range. These x-regions (with ≤50 meV/at differences between the polynomial fits to the cubic and wurtzite-type data points) are 0.3—0.75 for $Mo_{1-x}Al_xN$, 0.3—0.6 for $Mo_{1-x}Al_xN_{0.5(1+x)}$, and 0.55—0.8 for $Mo_{1-x}Al_xN_{0.5}$, see the vertical dashed lines within Fig. 1a, b, and c, respectively, Consequently, within these Al-contents, the preference for cubic or wurtzite-type phases is very sensitive to small changes in structure and atomic arrangements.

Our *ab initio* data clearly suggest increasing Al-solubility of the cubic phase with increasing N-vacancy content, Fig. 1a, b, and c, respectively. Therefore, we have selected the relatively low N_2-to-total pressure ratio of 0.32 during sputtering of our $Mo_{1-x}Al_xN_y$ coatings, which guaranties the formation of single-phase cubic-structured $MoN_{0.5}$ [1]. For lower nitrogen partial pressures, the Mo—N coatings also contain metallic Mo-based phases and for higher nitrogen partial pressures, the N-vacancy concentration decreases.

The nitrogen content of our sputtered $Mo_{1-x}Al_xN_y$ coatings increases nearly linearly from 35 to 49 at% with increasing Al-content x from 0 to 0.79, following the $MoN_{0.5}$—AlN quasi-binary tie line, see Fig. 2. Thus, the relationship between y and x can be described with $y = 0.5(1 + x)$ and $Mo_{1-x}Al_xN_{0.5(1+x)}$ solid solutions are formed, corresponding to the results obtained for $Mo_{1-x}Cr_xN_{0.5(1+x)}$ [1]. This chemical variation suggests that the theoretical vacancy content of the nitrogen sublattice continuously decreases from 50% ($MoN_{0.5}$) to 0% (AlN) when Al substitutes for Mo.

XRD analyses prove that our $Mo_{1-x}Al_xN_y$ coatings crystallize in a face-centered cubic structure with preferred (200)-orientation for Al/(Mo + Al)-ratios up to ~0.57, see Fig. 3a. Higher aluminum contents energetically prefer the formation of wurtzite-type $Mo_{1-x}Al_xN_y$ solid solutions. Both phases, cubic and wurtzite-type $Mo_{1-x}Al_xN_y$ coexist with x between 0.67 and 0.79, and the coating is predominantly wurtzite-type structured (with traces of the cubic phase) for $x = 1$. Fig. 3b is the corresponding color-coded XRD intensity map, based on our 13 different $Mo_{1-x}Al_xN_y$ coatings. This graphical representation is obtained by using a linear interpolation scheme between the experimentally obtained XRD patterns.

The stress-free lattice parameters of the experimentally obtained single-phased cubic-structured $Mo_{1-x}Al_xN_y$ coatings only slightly decrease from 4.18 ± 0.02 to 4.16 ± 0.02 Å with increasing Al-content x from 0 to 0.57, see Fig. 4. The comparison with the *ab initio* obtained averaged lattice parameters of face-centered cubic solid solutions along the three quasi-binary tie lines, MoN—AlN (1),
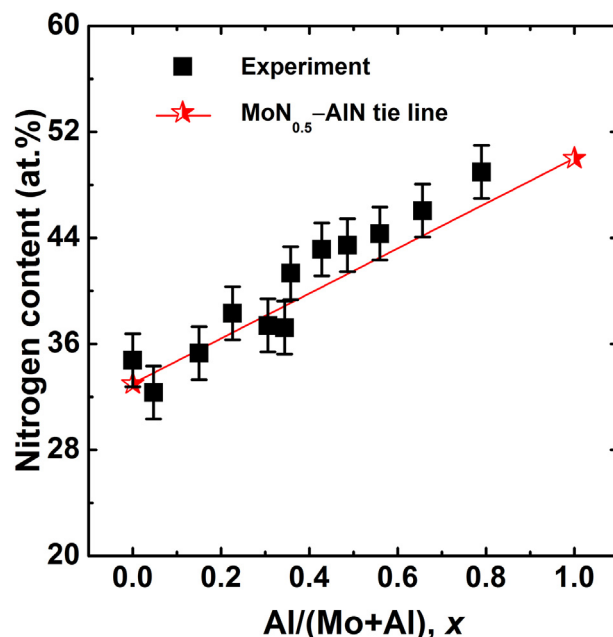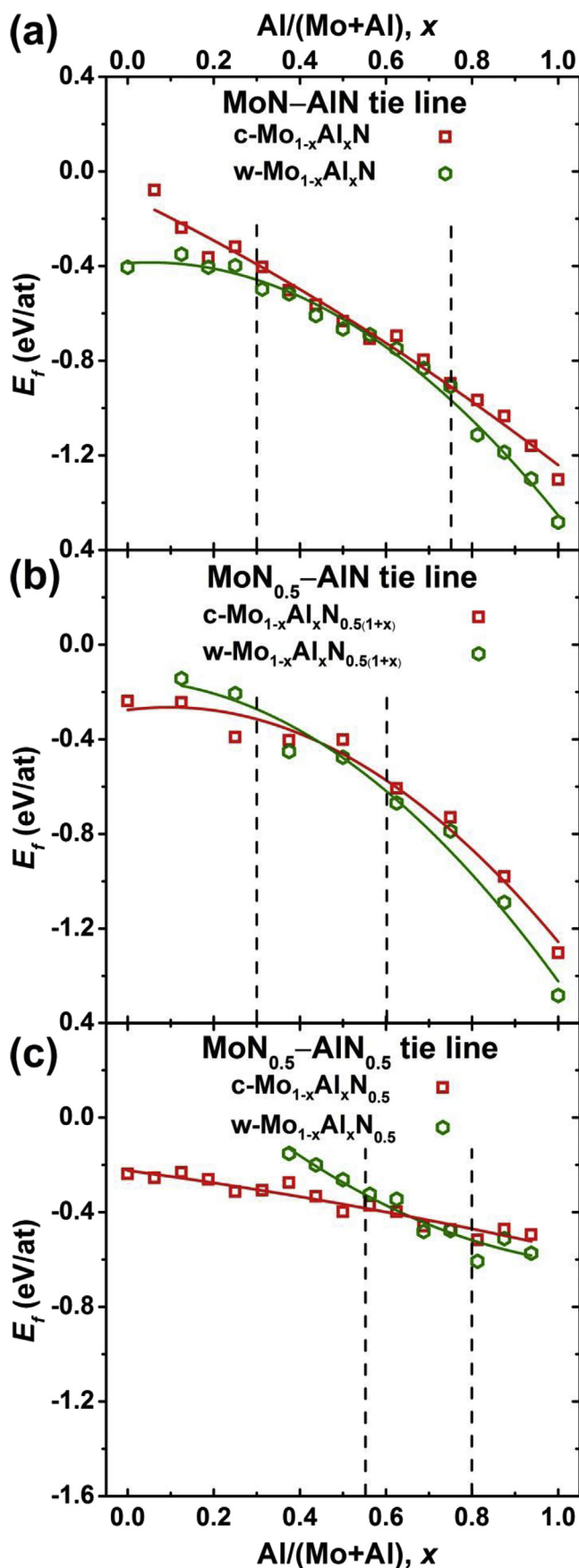
Fig. 2. Nitrogen content of our sputtered $Mo_{1-x}Al_xN_y$ coatings as a function of their Al-content, x.

MoN$_{0.5}$−AlN (2), and MoN$_{0.5}$−AlN$_{0.5}$ (3), shows an almost identical behavior with MoN$_{0.5}$−AlN (2) quasi-binary tie line. This suggests again (in addition to EDS analyses, Fig. 2) that c-Mo$_{1-x}$Al$_x$N$_{0.5(1+x)}$ solid solutions are formed. Only these c-Mo$_{1-x}$Al$_x$N$_{0.5(1+x)}$ struc-tures (along the MoN$_{0.5}$−AlN (2) quasi-binary tie line) provide lattice parameters with only a small dependence on the Al-content, comparable to the experimental data. This nearly unaltered lattice parameter, despite the replacement of large Mo atoms by small Al atoms, results from the counter-balance by additional nitrogen atoms. In contrast, the calculated lattice parameters for the vacancy-free c-Mo$_{1-x}$Al$_x$N solid solutions (along the MoN−AlN (1) quasi-binary tie line), as one might expect, decrease continuously with increasing Al-concentration, but also do not obey the linear Vegard's rule.

SEM investigations of fracture cross-sections of our coatings, Fig. 5, clearly show dense columnar growth morphologies, espe-cially for the single-phased c-Mo$_{1-x}$Al$_x$N$_{0.5(1+x)}$ coatings with $x \leq 0.57$. The column boundaries are less defined for coatings with x between 0.57 and 0.79, containing cubic and wurtzite-type phases as presented above, see Fig. 3. The single-phase wurtzite-type structured coatings, with $x = 0.79$ and 1, exhibit a fine fibrous growth morphology and strongly reduced coating thicknesses due to the pronounced reduction in deposition rate with increasing Al-content. The deposition rate estimated from the cross-section im-ages is with about 1.25 nm/s (for Al-contents x below 0.25) rela-tively high, but significantly decreases to ~0.2 nm/s (for w-AlN with traces of the cubic phase) with increasing x, see Fig. 6. The reduction in deposition rate with increasing Al-content is mainly based on the

Fig. 1. First principle calculations of the energy of formation, E$_f$, for cubic and wurtzite-type Mo$_{1-x}$Al$_x$N$_y$ along the quasi-binary tie lines MoN−AlN (a), MoN$_{0.5}$−AlN (b), and MoN$_{0.5}$−AlN$_{0.5}$ (c). Red squares and green hexagons represent E$_f$ of cubic and wurtzite-type structures, respectively. The colored solid lines represent second order poly-nomial fits of the individual data points. The vertical, dashed lines indicate the regions with ≤50 meV/at differences between these fits for cubic and wurtzite-type phases. (For interpretation of the references to color in this figure legend, the reader is referred to the web version of this article.)
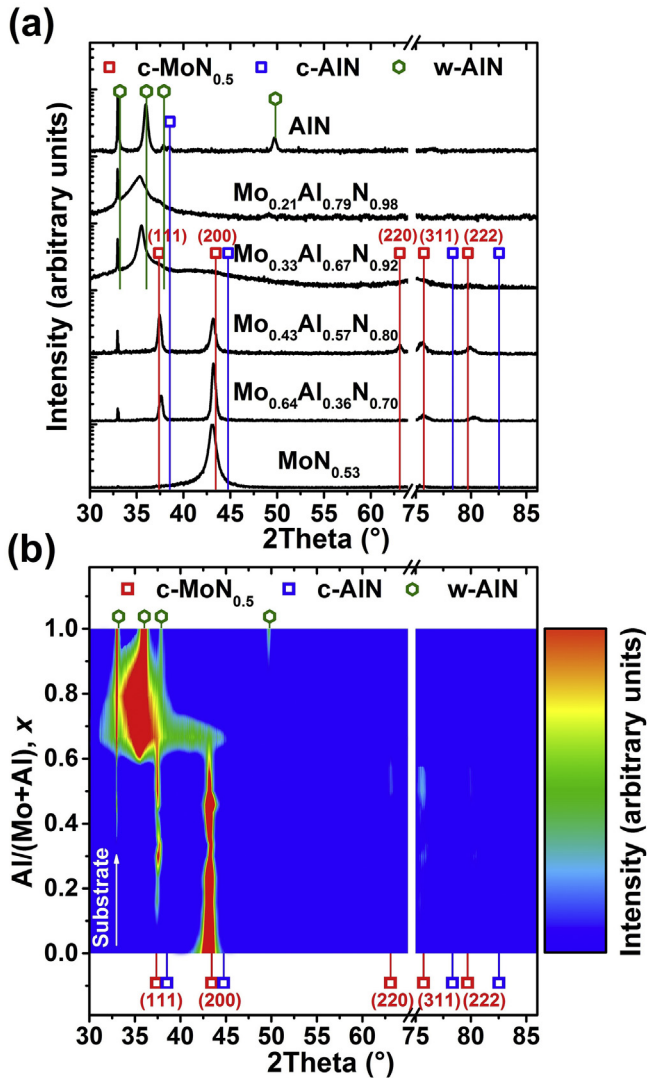
Fig. 3. The logarithmic-scaled XRD patterns of significant $Mo_{1-x}Al_xN_y$ coatings (a) and color-coded XRD intensities of all $Mo_{1-x}Al_xN_y$ coatings (b) with indicated peak positions for c-$MoN_{0.5}$ (ICDD 00-025-1366), c-AlN (ICDD 00-046-1200), and w-AlN (ICDD 00-025-1133). The narrow reflex at $2\theta \approx 33°$ corresponds to the Si-substrate (the second order diffraction). (For interpretation of the references to color in this figure legend, the reader is referred to the web version of this article.)

increasing poisoning effect of the target material, because AlN has a significantly lower conductivity as the Mo–N phases formed at the target surface.

The nanoindentation hardnesses, H, of our face-centered cubic c-$Mo_{1-x}Al_xN_{0.5(1+x)}$ coatings increases from ~33 to 38 GPa with increasing Al-content, see Fig. 7. The highest hardness (38.3 ± 1.7 GPa) of all coatings studied is obtained for c-$Mo_{0.43}Al_{0.57}N_{0.80}$ — the single-phase cubic-structured coating with the highest Al-content. The hardnesses of the coatings containing hexagonal wurtzite-type phases are between 22 and 25 GPa.

The indentation moduli of our single-phase cubic-structured coatings are between 410 and 480 GPa, but decrease to ~245 GPa for coatings containing hexagonal wurtzite-type phases Hence, their dependence on composition and crystal structure is very similar to the hardness evolution.

4. Discussion

Chemical analyses of our sputtered $Mo_{1-x}Al_xN_y$ coatings (Fig. 2)
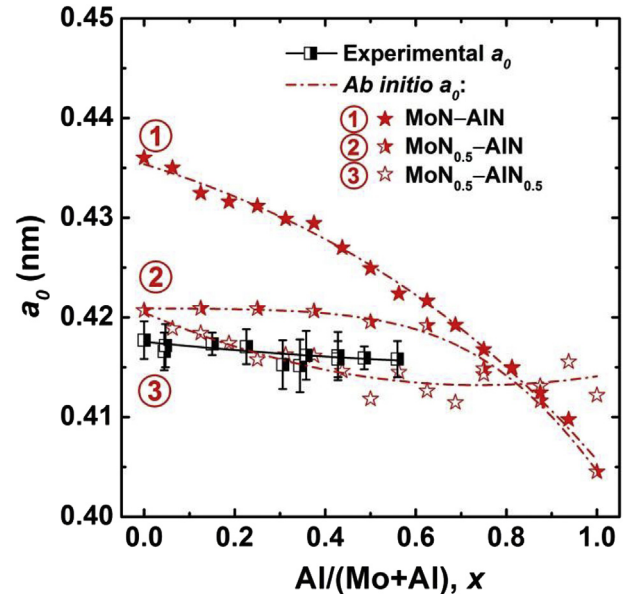
Fig. 4. Stress-free lattice parameters, a_0, of single-phased cubic-structured c-$Mo_{1-x}Al_xN_y$ coatings and cubic-structured solid solutions, $Mo_{1-x}Al_xN$, $Mo_{1-x}Al_xN_{0.5(1+x)}$, and $Mo_{1-x}Al_xN_{0.5}$, along the MoN–AlN (1), $MoN_{0.5}$–AlN (2), and $MoN_{0.5}$–$AlN_{0.5}$ (3) quasi-binary tie lines, respectively.

in combination with their structural investigations (Fig. 3a and b) suggest that cubic-structured $Mo_{1-x}Al_xN_y$ solid solutions are formed for Al-contents $x \leq 0.57$. Whereas $Mo_{0.43}Al_{0.57}N_{0.80}$ is still single-phase cubic-structured, $Mo_{0.33}Al_{0.67}N_{0.92}$ already contains wurtzite-type phases, and $Mo_{0.21}Al_{0.79}N_{0.98}$ is already single-phase wurtzite-type structured, compare Fig. 3a and b. With increasing Al-content, x, the N-content, y, also increases with a close to linear dependence following $y = 0.5(1 + x)$. Thus, the chemical composition of the solid solutions is best described by c-$Mo_{1-x}Al_xN_{0.5(1+x)}$, i.e. along the $MoN_{0.5}$–AlN quasi-binary tie line. The N-sublattice of their NaCl-type cubic structure is only half-populated for $MoN_{0.5}$ (hence, 50% of the N-sites are vacant), but fully populated for AlN. Consequently, the substitution of Mo by Al leads to a reduction in N-vacancies.

In excellent agreement with these chemical results, also the stress-free lattice parameters of our cubic-structured coatings can best be described by *ab initio* calculations along the $MoN_{0.5}$–AlN quasi-binary tie line, Fig. 4. The small but nearly constant overestimation of ~0.7% by *ab initio* is a well-known shortcoming of GGA [26]. The experimental and computational lattice parameters of c-$Mo_{1-x}Al_xN_{0.5(1+x)}$ only slightly decrease with increasing Al-content, because simultaneously also the vacant N-sites are filled. Contrary, the *ab initio* obtained lattice parameters of c-$Mo_{1-x}Al_xN_{0.5}$ and especially c-$Mo_{1-x}Al_xN$ solid solutions significantly decrease with increasing Al-content, because, their N-sublattice is unchanged when Al substitutes for Mo.

The maximum Al-content of $x = 0.57$, within our single-phase cubic-structured $Mo_{1-x}Al_xN_y$ coatings, excellently agrees with *ab initio* calculations of $Mo_{1-x}Al_xN_{0.5(1+x)}$ solid solutions. The latter exhibit Al-dependent N-vacancies along the $MoN_{0.5}$–AlN quasi-binary tie line, and energetically prefer the cubic structure for $x \leq 0.45$. Furthermore, the wurtzite-type phase is energetically preferred by only ≤ 50 meV/at for x between 0.45 and 0.6. $Mo_{1-x}Al_xN_{0.5}$ solid solutions, with constantly 50% vacant N-sites, favor the cubic structure up to even ~0.65. $Mo_{1-x}Al_xN$ solid solutions (with a fully populated N-sublattice), on the other hand, prefer the wurtzite-type structure across the whole composition range. These
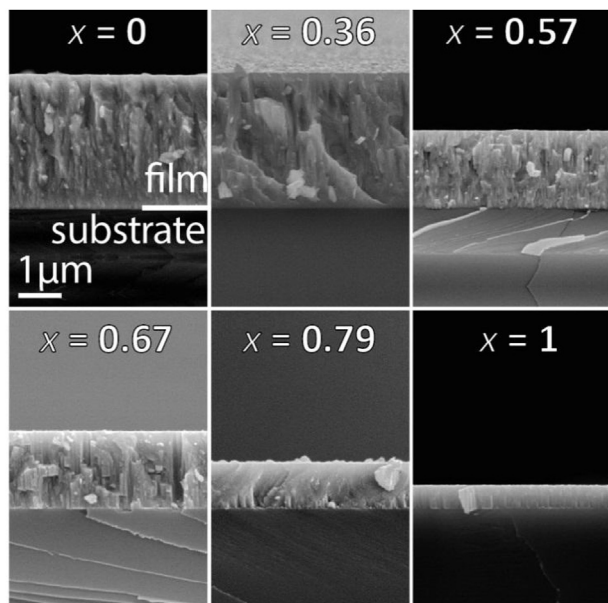
Fig. 5. SEM fracture cross-sections of significant $Mo_{1-x}Al_xN_y$ coatings with Al/(Mo + Al)-ratios, x, at the borders of the cubic (x = 0 and 0.57) and within the cubic phase region (x = 0.36) as well as $Mo_{1-x}Al_xN_y$ coatings, containing wurtzite-type phases (x = 0.67, 0.79 and 1).
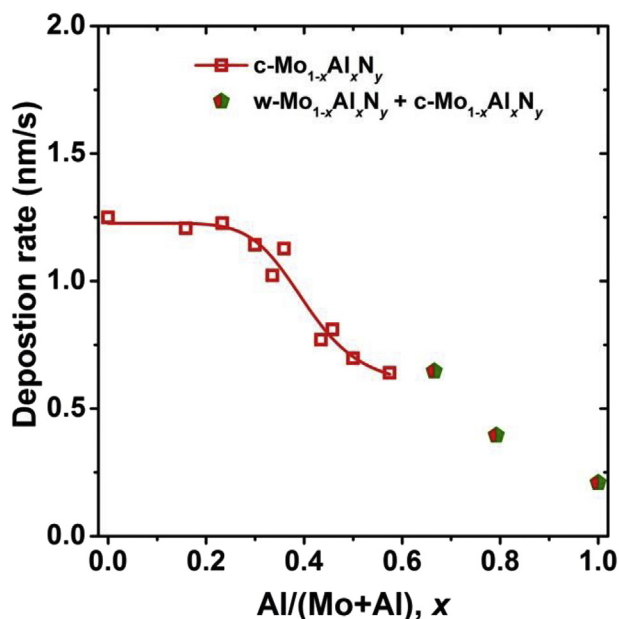
Fig. 6. Deposition rate of our $Mo_{1-x}Al_xN_y$ coatings as a function of their Al-content, x.

results suggest that N-vacancies support the formation of the cubic structure and allow for increased Al-contents within energetically preferred cubic-structured solid solutions.

The importance to stabilize the cubic structure within our $Mo_{1-x}Al_xN_y$ coatings up to high Al-contents is well represented by their mechanical properties, see Fig. 7. The hardness of single-phase cubic-structured $Mo_{1-x}Al_xN_{0.5(1+x)}$ coatings is always above 33 GPa and increases from 33.0 ± 1.7 GPa (for c-$MoN_{0.53}$) to 38.3 ± 1.7 GPa (for c-$Mo_{0.43}Al_{0.57}N_{0.80}$) with increasing Al-content. As soon as wurtzite-type $Mo_{1-x}Al_xN_y$ phases are formed, the hardness drops to only ~22 GPa.
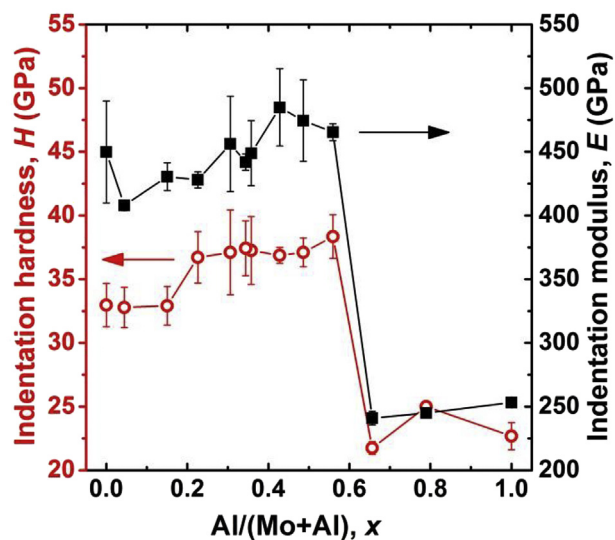
Fig. 7. Indentation hardness, H, (left axis, red open circles) and indentation modulus, E, (right axis, black solid squares) of our $Mo_{1-x}Al_xN_y$ coatings as a function of their Al-content, x. (For interpretation of the references to color in this figure legend, the reader is referred to the web version of this article.)

Our *ab initio* and experimental studies suggest, that the high nitrogen partial pressure used during deposition of $Mo_{1-x}Al_xN_y$ thin films, as reported in Refs. [17,18], is responsible for the observed maximum Al/(Mo + Al)-ratio of ~0.3 within cubic-structured coatings and the general hardness-decrease with increasing Al-content. Considering the additional chemical potential of nitrogen, a high nitrogen pressure within the deposition chamber favors the formation of a fully occupied N-sublattice, hence, $Mo_{1-x}Al_xN$ solid solutions. Contrary, a nitrogen-deficient atmosphere supports the formation of N-vacancies, hence, $Mo_{1-x}Al_xN_{0.5(1+x)}$ and $Mo_{1-x}Al_xN_{0.5}$ solid solutions. Thus, a low nitrogen partial pressure allows to increase the maximum Al-content within the cubic structure, cf. Fig. 1.

5. Summary and conclusions

Ab initio calculations of solid solutions along the three quasi-binary tie lines, $MoN–AlN$, $MoN_{0.5}–AlN$, and $MoN_{0.5}–AlN_{0.5}$, clearly show that the chemical stability range of the cubic structure increases (on the expanse of wurtzite-type structure) when N-vacancies are present. Whereas for $Mo_{1-x}Al_xN$ solid solutions (theoretically having no N-vacancies) the wurtzite-type structure is preferred across the entire composition range, cubic-structured c-$Mo_{1-x}Al_xN_{0.5(1+x)}$ and c-$Mo_{1-x}Al_xN_{0.5}$ solid solutions are energetically favorable even up to significantly increased Al-concentrations. Based on these results, we have chosen a low N_2-to-total pressure ratio $p_{N2}/p_T = 0.32$ for the preparation of $Mo_{1-x}Al_xN_y$ coatings. This allows the development of single-phase cubic-structured c-$Mo_{1-x}Al_xN_y$ solid solutions up to Al-contents of x ~0.57, currently the highest value reported for c-$Mo_{1-x}Al_xN_y$. With higher Al-contents, also wurtzite-type phases are formed and for x ≥ 0.79 the coatings predominantly crystallize within the wurtzite-type structure.

Combined with structural investigations, detailed chemical studies show that the N-content, y, of our c-$Mo_{1-x}Al_xN_y$ solid solutions continuously increases from ~0.53 to 0.80 with increasing Al-content from x = 0 to ~0.57. Consequently, their chemical composition follows the $MoN_{0.5}–AlN$ quasi-binary tie line, and can thus best be described as $Mo_{1-x}Al_xN_{0.5(1+x)}$, indicating that the ~50% nitrogen vacancies present in $MoN_{0.5}$ are filled (with N) when Al

substitutes for Mo.

Ab initio calculations highlight that with increasing vacancy content at the nitrogen sublattice the transition from c-$Mo_{1-x}Al_xN_y$ to w-$Mo_{1-x}Al_xN_y$ shifts to higher Al-contents. The importance of maintaining the cubic structure within this material system is well represented by the hardness of our films. With increasing Al-content, the hardness increases from ~33 GPa (for c-$MoN_{0.53}$) to 38 GPa (for c-$Mo_{0.43}Al_{0.57}N_{0.80}$) as long as the coatings are single-phase cubic-structured, but drops to ~22 GPa for phase wurtzite-type structured the coatings with higher Al-contents, containing hexagonal wurtzite-type phases.

Based on our detailed *ab initio* calculations in combination with experimental studies we can conclude that nitrogen vacancies (or vacancies in general) have a significant and determining role for the stabilization of various phases. Within the Mo−Al−N material system, nitrogen vacancies are essential to stabilize the cubic structure up to very high Al-contents, which are necessary pre-requisites for high thermal stability and strength.

Acknowledgments

References

[1] F.F. Klimashin, H. Riedl, D. Primetzhofer, J. Paulitsch, P.H. Mayrhofer, Composition driven phase evolution and mechanical properties of Mo−Cr−N hard coatings, J. Appl. Phys. 118 (2015) 025305.
[2] M. Ürgen, O. Eryilmaz, A. Cakir, E. Kayali, B. Nilüfer, Y. Işik, Characterization of molybdenum nitride coatings produced by arc-PVD technique, Surf. Coat. Technol. 94 (1997) 501−506.
[3] G. Gassner, P.H. Mayrhofer, K. Kutschej, C. Mitterer, M. Kathrein, Magnéli phase formation of PVD Mo−N and W−N coatings, Surf. Coat. Technol. 201 (2006) 3335−3341.
[4] P.H. Mayrhofer, A. Hörling, L. Karlsson, J. Sjölén, T. Larsson, C. Mitterer, L. Hultman, Self-organized nanostructures in the Ti-Al-N system, Appl. Phys. Lett. 83 (2003) 2049−2051.
[5] C. Wüstefeld, D. Rafaja, V. Klemm, C. Michotte, M. Kathrein, Effect of the aluminium content and the bias voltage on the microstructure formation in Ti 1− x Al x N protective coatings grown by cathodic arc evaporation, Surf. Coat. Technol. 205 (2010) 1345−1349.
[6] D. McIntyre, J. Greene, G. Håkansson, J.E. Sundgren, W.D. Münz, Oxidation of metastable single-phase polycrystalline Ti0. 5Al0. 5N films: Kinetics and mechanisms, J. Appl. Phys. 67 (1990) 1542−1553.
[7] V. Anikin, I. Blinkov, A. Volkhonskii, N. Sobolev, S. Tsareva, R. Kratokhvil, A. Frolov, Ion-plasma Ti-Al-N coatings on a cutting hard-alloy tool operating under conditions of constant and alternating-sign loads, Russ. J. Non-Ferrous Metals 50 (2009) 424−431.
[8] H. Willmann, P. Mayrhofer, P.Å. Persson, A. Reiter, L. Hultman, C. Mitterer, Thermal stability of Al−Cr−N hard coatings, Scr. Mater. 54 (2006) 1847−1851.
[9] K. Bobzin, E. Lugscheider, R. Nickel, N. Bagcivan, A. Krämer, Wear behavior of Cr 1− x Al x N PVD-coatings in dry running conditions, Wear 263 (2007) 1274−1280.
[10] Q. Xia, H. Xia, A.L. Ruoff, Pressure-induced rocksalt phase of aluminum nitride: A metastable structure at ambient condition, J. Appl. Phys. 73 (1993) 8198−8200.
[11] S. PalDey, S. Deevi, Single layer and multilayer wear resistant coatings of (Ti, Al) N: a review, Mater. Sci. Eng. A 342 (2003) 58−79.
[12] P. Mayrhofer, D. Music, J. Schneider, Ab initio calculated binodal and spinodal of cubic Ti Al x N, Appl. Phys. Lett. 88 (2006) 071922.
[13] D. Holec, F. Rovere, P.H. Mayrhofer, P.B. Barna, Pressure-dependent stability of cubic and wurtzite phases within the TiN−AlN and CrN−AlN systems, Scr. Mater. 62 (2010) 349−352.
[14] A. Sugishima, H. Kajioka, Y. Makino, Phase transition of pseudobinary Cr−Al−N films deposited by magnetron sputtering method, Surf. Coat. Technol. 97 (1997) 590−594.
[15] P.H. Mayrhofer, D. Music, T. Reeswinkel, H.G. Fuß, J.M. Schneider, Structure, elastic properties and phase stability of Cr1−xAlxN, Acta Mater. 56 (2008) 2469−2475.
[16] J. Šůna, J. Musil, P. Dohnal, Control of macrostress σ in reactively sputtered Mo−Al−N films by total gas pressure, Vacuum 80 (2006) 588−592.
[17] J. Yang, Z. Yuan, Q. Liu, X. Wang, Q. Fang, Characterization of Mo−Al−N nanocrystalline films synthesized by reactive magnetron sputtering, Mater. Res. Bull. 44 (2009) 86−90.
[18] J. Xu, H. Ju, L. Yu, Microstructure, oxidation resistance, mechanical and tribological properties of Mo−Al−N films by reactive magnetron sputtering, Vacuum 103 (2014) 21−27.
[19] G. Kresse, J. Furthmüller, Efficient iterative schemes for ab initio total-energy calculations using a plane-wave basis set, Phys. Rev. B 54 (1996) 11169.
[20] G. Kresse, J. Hafner, Ab initio molecular dynamics for liquid metals, Phys. Rev. B 47 (1993) 558.
[21] H. Euchner, P. Mayrhofer, Vacancy-dependent stability of cubic and wurtzite Ti 1− x AlxN, Surf. Coat. Technol. 275 (2015) 214−218.
[22] A. Van de Walle, P. Tiwary, M. De Jong, D. Olmsted, M. Asta, A. Dick, D. Shin, Y. Wang, L.-Q. Chen, Z.-K. Liu, Efficient stochastic generation of special quasirandom structures, Calphad 42 (2013) 13−18.
[23] D. Rafaja, C. Wüstefeld, C. Baehtz, V. Klemm, M. Dopita, M. Motylenko, C. Michotte, M. Kathrein, Effect of internal interfaces on hardness and thermal stability of nanocrystalline Ti0. 5Al0. 5N coatings, Metallurgical Mater. Trans. A 42 (2011) 559−569.
[24] W.C. Oliver, G.M. Pharr, An improved technique for determining hardness and elastic modulus using load and displacement sensing indentation experiments, J. Mater. Res. 7 (1992) 1564−1583.
[25] A.C. Fischer-Cripps, Critical review of analysis and interpretation of nanoindentation test data, Surf. Coat. Technol. 200 (2006) 4153−4165.
[26] A. Khein, D.J. Singh, C.J. Umrigar, All-electron study of gradient corrections to the local-density functional in metallic systems, Phys. Rev. B 51 (1995) 4105.